Sonic-Point Capturing

Bram van Leer*
Wen-Tzong Lee†
and
Kenneth G. Powell‡

The University of Michigan
Department of Aerospace Engineering

1 Introduction

The ability of conservative, dissipative difference schemes to capture shocks in discrete flow solutions is much appreciated and fairly well understood. Some unresolved issues in shock capturing concern the existence and uniqueness of steady shock structures [1,2], numerical noise radiated by captured shocks [3,4,5], and rotationally invariant shock capturing [6,7]. All of these arise from pursuing the narrowest possible shock profile under all circumstances, and hardly detract from the utility of the technique.

Less understood, but no less of a miracle, is the ability of difference schemes to capture sonic points in discrete solutions, especially in steady solutions, where the transition through a sonic point marks a bifurcation. In quasi-one-dimensional nozzle flow, for example, the transonic solution is an isolated solution of the boundary-value problem: perturbing the inflow Mach number renders the solution either fully subsonic or unsteady.

Steady numerical solutions containing sonic points may exhibit a variety of oddities. If the discrete scheme does not recognize the entropy condition, i.e., if it admits expansion shocks, an arbitrarily large jump may be found where one expects a smooth transition through the sonic point [8]; if it does, the solution may still exhibit a jump of magnitude $O(\Delta x)$ [9], or a two-cell plateau (see below), or anything in between, in addition to being non-unique and slow to converge. The small transonic jump, in particular, can be found in numerous published flow solutions obtained with first-order upwind methods [3,10]; higher-order upwind methods, though, if patterned after the MUSCL scheme [11], are insensitive to the presence of a sonic point.

In what follows we shall derive and test a prototype scheme that produces perfectly smooth transonic solutions to nozzle-flow problems, without recourse to heavy-duty artificial dissipation. Most of the pieces of the transonic puzzle have been carried on by others, viz. Harten [12], Roe (as reported in [8]), and Goodman and LeVeque [13]; the missing piece is produced here. The secret of success lies in treating the source term in the same way as the flux-derivative term; this has the appearance of applying an entropy fix to the source term. In reality all that is done is balancing the flux derivative and the source term in both forward- and backward-moving parts of the transonic expansion fan.

*Professor, Member AIAA
†Graduate Research Assistant
‡Assistant Professor, Member AIAA

2 Basic upwind scheme

Our starting point is the first-order upwind-differencing scheme of Roe[14] and Van Leer [8] for a hyperbolic system of equations incorporating a source term:

$$u_t + f_x = s; \tag{1}$$

to fix our thoughts we shall think of this equation as representing the quasi-one-dimensional Euler equations for flow in a duct with a variable cross-section $D(x)$. A steady transition from subsonic to supersonic flow can only occur when $D'(x) = 0$, $D''(x) > 0$, i.e., in a throat.

The difference scheme can be written as

$$u_i^{n+1} = u_i^n - \frac{\Delta t}{\Delta x}\left(f_{i+\frac{1}{2}}^n - f_{i-\frac{1}{2}}^n\right) + \frac{\Delta t}{2}\left(\hat{s}_{i-\frac{1}{2}}^n + \hat{s}_{i+\frac{1}{2}}^n\right), \tag{2}$$

in which the numerical flux function $f_{i+\frac{1}{2}}$ is defined as

$$\begin{aligned} f_{i+\frac{1}{2}} &\equiv f(u_i, u_{i+1}) \\ &= \frac{1}{2}[f(u_i) + f(u_{i+1})] \\ &\quad -\frac{1}{2}\left[|\hat{A}|_{i+\frac{1}{2}}(u_{i+1} - u_i) - |\hat{s}|_{i+\frac{1}{2}}\Delta x\right]; \end{aligned} \tag{3}$$

the notation requires further explanation.

- $df/du = A = R\Lambda R^{-1}$, where $\Lambda \equiv diag(a_k)$ carries the characteristic speeds in the diagonal;

- $|A| = R|\Lambda|R^{-1}$ with

$$|\Lambda| \equiv diag\,(|a_k|)\,; \tag{4}$$

also useful are the definitions

$$A^{\pm} = R\Lambda^{\pm}R^{-1}, \quad \Lambda^{\pm} = diag\,(a_k^{\pm})\,, \tag{5}$$

and the relations

$$A^{+} + A^{-} = A, \quad A^{+} - A^{-} = |A|; \tag{6}$$

- $|s| = \sum |z_k| R_k$ follows after writing $s = Rz = \sum z_k R_k$, i.e., expressing s in terms of the right eigenvectors of A; other useful definitions are

$$s^{\pm} = \sum_k z_k^{\pm} R_k, \tag{7}$$

with

$$s^{+} + s^{-} = s, \quad s^{+} - s^{-} = |s|; \tag{8}$$

- $\hat{A}_{i+\frac{1}{2}} \equiv A(\hat{u}_{i+\frac{1}{2}})$, where $\hat{u}_{i+\frac{1}{2}} \equiv \hat{u}(u_i, u_{i+1})$ is the Roe average [14] of u_i and u_{i+1}; similarly, $\hat{s}_{i+\frac{1}{2}} \equiv s(\hat{u}_{i+\frac{1}{2}})$.

With the above flux function the full scheme (2) can be written in a form that shows its upwind character:

$$\begin{aligned} u_i^{n+1} &= u_i^n \\ &\quad -\frac{\Delta t}{\Delta x}\left(\left[\hat{A}^{+}_{i-\frac{1}{2}}(u_i - u_{i-1}) - \hat{s}^{+}_{i-\frac{1}{2}}\Delta x\right]^n\right. \\ &\quad \left. + \left[\hat{A}^{-}_{i+\frac{1}{2}}(u_{i+1} - u_i) - \hat{s}^{-}_{i+\frac{1}{2}}\Delta x\right]^n\right). \end{aligned} \tag{9}$$

Note that both the flux difference and the source term are split to achieve upwind bias. Although a first-order time-stepping scheme, (9) becomes second-order accurate when the solution becomes steady: each flux difference is centered on the same interval as the source term that must balance it. Eq (9) can further be expanded as

$$\begin{aligned} u_i^{n+1} &= u_i^n \\ &\quad -\frac{\Delta t}{\Delta x}\left(\sum_{\hat{a}_k \geq 0}\left[\hat{R}_k\left(\hat{a}_k\Delta v_k - \hat{z}_k\Delta x\right)\right]^n_{i-\frac{1}{2}}\right. \\ &\quad \left. + \sum_{\hat{a}_k < 0}\left[\hat{R}_k\left(\hat{a}_k\Delta v_k - \hat{z}_k\Delta x\right)\right]^n_{i+\frac{1}{2}}\right); \end{aligned} \tag{10}$$

here we have introduced the characteristic variables v defined by

$$dv = Rdu. \tag{11}$$

In a steady state without shocks we have

$$(\hat{a}_k\Delta v_k - \hat{z}_k\Delta x)_{i+\frac{1}{2}} = 0 \tag{12}$$

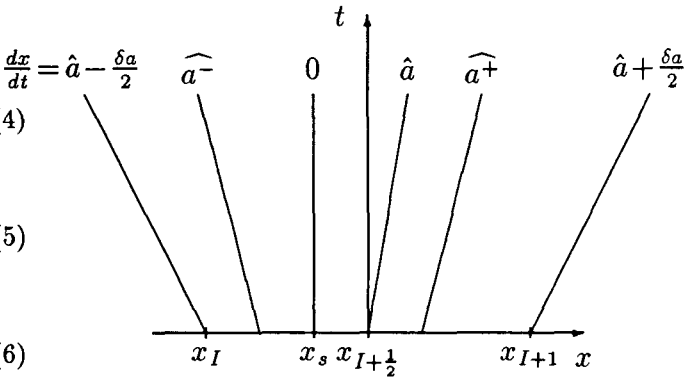

Figure 1a: Geometry of transonic expansion fan: space-time diagram.

for each k at each interface $x_{i+\frac{1}{2}}$.

The scheme thus formulated does not contain an "entropy fix", i.e., a special measure to break down expansion shocks. Suppose that in cell I there is a sonic point in the $k-$th characteristic field, i.e.

$$(a_k)_{I-\frac{1}{2}} < 0 < (a_k)_{I+\frac{1}{2}}, \tag{13}$$

then the v_k-component in u_I, i.e., the component along R_k, is not updated, as seen from (10). This is the reason why an initially present expansion discontinuity may not decay. In the next section we shall discuss how to modify the flux function in order to prevent such unphysical behavior.

3 Satisfying the Entropy Condition

To satisfy the entropy condition we merely have to build into the flux formula the model of a smooth transonic expansion wave; this will generate a small artificial viscosity of a special functional form.

Assume, therefore, we have a characteristic field with a sonic point between x_I and x_{I+1}; we shall approximate the spatial variation of the characteristic speed by a linear distribution, as shown in Figure 1. In the following derivation, the subscript k is suppressed for clarity. In the transonic expansion fan between x_I and x_{I+1} various average characteristic speeds can be recognized:

- $\hat{a}$ $\equiv$ the average characteristic speed in the entire fan;
- $\widehat{a^+} \equiv$ the average positive characteristic speed in the fan;
- $\widehat{a^-} \equiv$ the average negative characteristic speed in the fan.

Because the averaging operation comes after taking the positive/negative part of a, the quantities $\widehat{a^{\pm}}$ do not

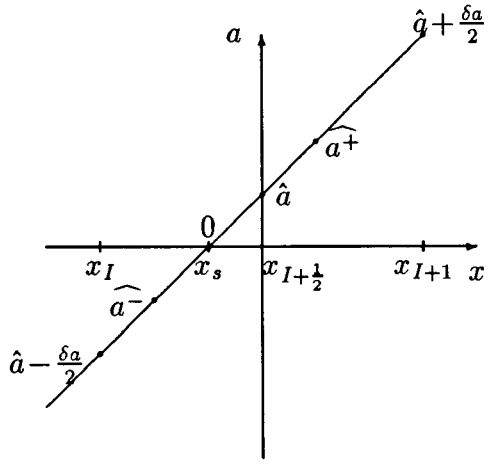

Figure 1b: Geometry of transonic expansion fan: a versus x.

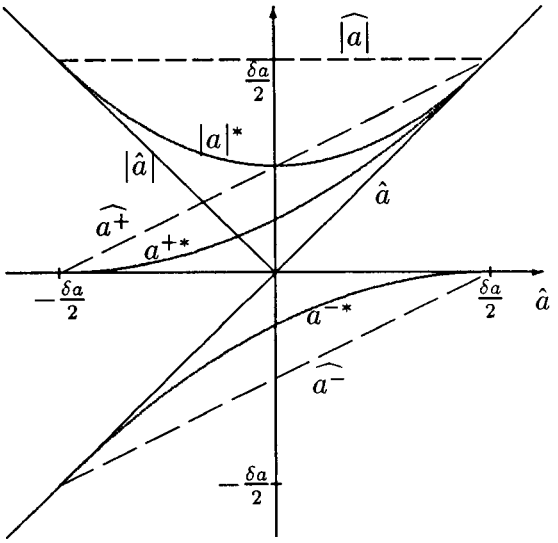

Figure 2: Functions of $\hat{a}$ and δa.

relate to $\hat{a}$ as usual, i.e.,

$$\widehat{a^+} \neq \hat{a}^+ \equiv max(\hat{a}, 0), \quad \widehat{a^-} \neq \hat{a}^- \equiv min(\hat{a}, 0), \quad (14)$$

but we still have

$$\widehat{a^+} + \widehat{a^-} = \hat{a}, \quad (15)$$

and we may introduce a consistent absolute value by defining

$$\widehat{|a|} = \widehat{a^+} - \widehat{a^-}, \quad (16)$$

which, however, does not equal the true average absolute characteristic speed in the fan. Introducing the spread δa of the characteristic speed across the fan, i.e.,

$$(\delta a)_{I+\frac{1}{2}} = a_{I+1} - a_I > 0, \quad (17)$$

we have the following expressions,

$$\widehat{a^\pm} = \frac{1}{2}(\hat{a} \pm \frac{\delta a}{2}), \quad \widehat{|a|} = \frac{\delta a}{2}, \quad (18)$$

valid in the transonic case $a_I < \hat{a} < a_{I+1}$, or

$$-\frac{\delta a}{2} < \hat{a} < \frac{\delta a}{2}. \quad (19)$$

We shall now determine the change of the characteristic quantity v across the forward- and backward-moving portions of the fan. Conservation and symmetry requirements dictate the following constraint:

$$\hat{a}\Delta v = \widehat{a^+}(\Delta v)^+ + \widehat{a^-}(\Delta v)^-. \quad (20)$$

Assuming that v changes linearly through the fan, we take Δv in proportion to the width of the forward/backward part of the fan, i.e.,

$$(\Delta v)^+ = \frac{\hat{a} + \frac{\delta a}{2}}{\delta a}\Delta v \quad (21a)$$

$$= \frac{2\widehat{a^+}}{\delta a}\Delta v \quad (21b)$$

$$(\Delta v)^- = -\frac{\hat{a} - \frac{\delta a}{2}}{\delta a}\Delta v \quad (21c)$$

$$= -\frac{2\widehat{a^-}}{\delta a}\Delta v. \quad (21d)$$

Using (21) to eliminate $(\Delta v)^\pm$, we may rewrite the splitting (20) as

$$\hat{a}\Delta v = a^{+*}\Delta v + a^{-*}\Delta v, \quad (22)$$

with

$$a^{+*} = 2\frac{(\widehat{a^+})^2}{\delta a}, \quad a^{-*} = -2\frac{(\widehat{a^-})^2}{\delta a}; \quad (23)$$

this, by construction, is an identity. The quantities $a^{\pm *}$ may be called the effective forward and backward characteristic speeds in the fan. As seen from (22), they still add up to $\hat{a}$,

$$a^{+*} + a^{-*} = \hat{a}, \quad (24)$$

and we may again introduce an effective absolute value:

$$|a|^* \equiv a^{+*} - a^{-*} = \frac{\hat{a}^2}{\delta a} + \frac{\delta a}{4}. \quad (25)$$

This is precisely the form of the modified absolute value proposed by Harten [12] as a replacement for $|\hat{a}|$ in Eq. (4), in order to circumvent the vanishing of $|\hat{a}|$ in a transonic expansion wave, which would mean vanishing dissipation and the possibility of an expansion shock. Harten's choice was simply a smooth fit to the standard absolute-value function (see Figure 2); the uniqueness of this choice, suggested by the above derivation, apparently has not been appreciated until now.

Even more surprising is that Godunov's [15] flux function, known to satisfy the entropy condition, can be implemented exactly, or in close approximation, by using (25). To understand this, we do best to consider the special case of the inviscid Burgers equation,

$$u_t + (\frac{1}{2}u^2)_x = 0, \tag{26}$$

in which the characteristic speed a equals u itself.

Godunov's flux is taken from the solution of Riemann's problem at the cell interface; in a transonic expansion this yields

$$f(u_I, u_{I+1}) = 0, \quad u_I < 0 < u_{I+1}. \tag{27}$$

Using our modified flux function

$$\begin{aligned} f(u_I, u_{I+1}) &= \frac{1}{4}(u_I^2 + u_{I+1}^2) \\ &\quad -\frac{1}{2}|u|^*_{I+\frac{1}{2}}(u_{I+1} - u_I), \end{aligned} \tag{28}$$

with

$$|u|^*_{I+\frac{1}{2}} = \left(\frac{\hat{u}^2}{\delta u} + \frac{\delta u}{4}\right)_{I+\frac{1}{2}}, \tag{29}$$

$$\hat{u}_{I+\frac{1}{2}} = \frac{1}{2}(u_I + u_{I+1}), \tag{30}$$

$$(\delta u)_{I+\frac{1}{2}} = u_{I+1} - u_I, \tag{31}$$

we find the same result:

$$\begin{aligned} f(u_I, u_{I+1}) &= \frac{1}{4}(u_I^2 + u_{I+1}^2) \\ &\quad -\frac{1}{8}\left[(u_I + u_{I+1})^2 + (u_{I+1} - u_I)^2\right] \\ &= 0. \end{aligned} \tag{32}$$

This flux function, as mentioned in the Introduction, produces a small jump across the sonic point. In an attempt to remedy this, Roe, as reported in [8], derived a transonic flux for Burgers' equation that is *negative*:

$$f(u_I, u_{I+1}) = \frac{1}{2}u_I u_{I+1}. \tag{33}$$

This formula, combined with the standard upwind flux away from the sonic point, achieves that

$$\frac{\partial u_{I+1}/\partial t}{\partial u_I/\partial t} = \frac{u_{I+1}}{u_I}, \tag{34}$$

which is exactly how a transonic expansion wave would evolve in reality, in the absence of a source.

The flux function (33) reaches its minimum when the sonic point falls exactly at $x_{I+\frac{1}{2}}$, i.e., when

$$u_I = -u_{I+1}; \tag{35}$$

the minimum flux value equals

$$f(-u_{I+1}, u_{I+1}) = -\frac{1}{2}u_{I+1}^2. \tag{36}$$

The same level of dissipation can be reached by the modified flux (28) if we *artificially* double the spread of the expansion fan, by redefining

$$(\delta u)_{I+\frac{1}{2}} = 2(u_{I+1} - u_I). \tag{37}$$

This leads to the transonic flux

$$f(u_I, u_{I+1}) = -\frac{1}{16}(u_I^2 + u_{I+1}^2) + \frac{3}{8}u_I u_{I+1}; \tag{38}$$

its minimum value is reached in the case of (35) and is given by (36).

At this point it is instructive to investigate how the standard upwind flux (3), without entropy fix, compares to (27) and (33) or (38). In the absence of a source term it reads

$$\begin{aligned} f(u_I, u_{I+1}) &= \frac{1}{4}(u_I^2 + u_{I+1}^2) \\ &\quad -\frac{1}{4}|u_I + u_{I+1}|(u_{I+1} - u_I) \end{aligned} \tag{39}$$

$$\begin{aligned} &= \min\left(\frac{1}{2}u_I^2, \frac{1}{2}u_{I+1}^2\right) \\ &\quad u_I < 0 < u_{I+1}, \end{aligned} \tag{40}$$

and reaches a maximum in case (35):

$$f(-u_{I+1}, u_{I+1}) = \frac{1}{2}u_{I+1}^2. \tag{41}$$

If we measure the amount of dissipation in a transonic flux as the difference between that flux and the above, dissipation-free reference flux (39), in the worst case (35), we see that Roe's formula (33), and the smooth version (38), have twice as much dissipation as Godunov's formula (27).

The amount of dissipation in (33) or (38) is still not enough to get a smooth transition through the sonic point; it needs to be doubled once more, as shown by Goodman and LeVeque [13]. In their analysis, the crucial point is to make the scheme for the transonic region consistent with a higher-order equation derived from the inviscid Burgers equation:

$$\frac{\partial^2 u}{\partial t \partial x} + \frac{\partial^2(\frac{1}{2}u^2)}{\partial x^2} = 0. \tag{42}$$

Expanding the second term yields

$$\frac{\partial^2 u}{\partial t \partial x} = -\left(\frac{\partial u}{\partial x}\right)^2 - u\frac{\partial^2 u}{\partial x^2}; \tag{43}$$

the second right-hand term can be neglected near the sonic point:

$$\frac{\partial^2 u}{\partial t \partial x} \approx -\left(\frac{\partial u}{\partial x}\right)^2, \quad u \approx 0. \tag{44}$$

Calling the unknown transonic flux f_t, and using the standard upwind flux at $x_{I-\frac{1}{2}}$ and $x_{I+\frac{3}{2}}$, we find that the first-order upwind scheme approximates (43) as

$$\frac{\partial}{\partial t}\left(\frac{u_{I+1}-u_I}{\Delta x}\right) = -\frac{1}{\Delta x}\left(\frac{\frac{1}{2}u_{I+1}^2 - f_t}{\Delta x} - \frac{f_t - \frac{1}{2}u_I^2}{\Delta x}\right); \quad (45)$$

upon comparing (45) with (44) we see that the former will be a consistent approximation to the latter if the transonic flux is chosen as

$$f_t = -\frac{1}{4}(u_I^2 + u_{I+1}^2) + u_I u_{I+1}. \quad (46)$$

The minimum of this flux again is reached in the case of (35), and equals

$$f_t(-u_{I+1}, u_{I+1}) = -\frac{3}{2}u_{I+1}^2, \quad (47)$$

four times as far away from the dissipation-free flux (39) as Godunv's flux (27), and twice as far as (33) or (38). The same dissipation level can be reached with our generic formula (28) by artificially doubling the spread of the transonic fan once more, i.e., by redefining

$$(\delta u)_{I+\frac{1}{2}} = 4(u_{I+1} - u_I). \quad (48)$$

A compact, scale-free way to represent flux formulas for Burgers' equation, due to Roe,is to define the angle variable θ,

$$\cos(\theta_{i+\frac{1}{2}}) = \frac{u_i}{\sqrt{u_i^2 + u_{i+1}^2}}, \quad (49a)$$

$$\sin(\theta_{i+\frac{1}{2}}) = \frac{u_{i+1}}{\sqrt{u_i^2 + u_{i+1}^2}}, \quad (49b)$$

and normalize the upwind flux by the central-differencing flux:

$$\phi(\theta_{i+\frac{1}{2}}) = \frac{f(u_i, u_{i+1})}{\frac{1}{4}(u_i^2 + u_{i+1}^2)}. \quad (50)$$

Figure 3 summarizes all the transonic fluxes mentioned before, the standard upwind flux, and two distinct fluxes used in a transonic compression shock ($u_I > 0 > u_{I+1}$), namely, Godunov's and Osher's [10]. From the viewpoint of implicit differencing it is desirable to have a numerical flux function that is differentiable with respect to the input states; this condition is met throughout by Osher's flux, and by the transonic fluxes of the family (28).

It has been known for some time [16] that Godunov's flux represents the border-line of fluxes satisfying the entropy condition. To understand this, consider a flux

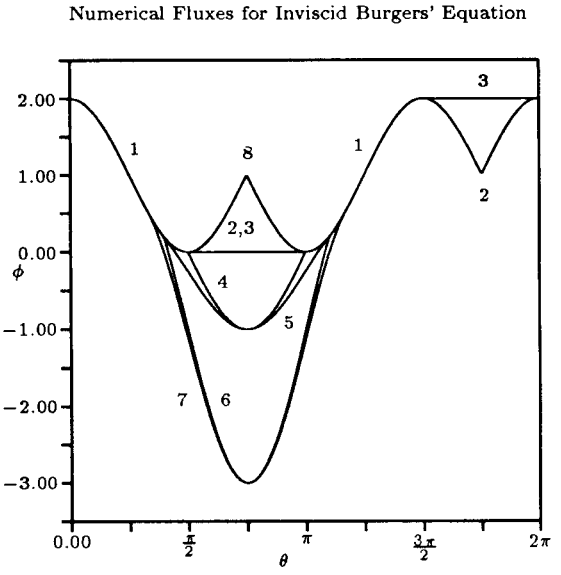

Figure 3: Dimensionless numerical fluxes for the inviscid Burgers equation.

1. Standard upwind flux, Eq. (39), away from transonic expansions and compressions
2. Godunov, Eq. (27), equivalent to Eqs. (28–30) with $\delta u = \Delta u$
3. Osher
4. Roe, Eq. (33)
5. Modified transonic flux, Eqs. (28-30), with $\delta u = 2\Delta u$
6. Goodman and LeVeque, Eq. (46)
7. Modified transonic flux with $\delta u = 4\Delta u$
8. Dissipation-free transonic flux, Eq. (39)

of the form (28), with an artificially *reduced* spread of the expansion fan:

$$(\delta u)_{I+\frac{1}{2}} < u_{I+1} - u_I. \tag{51}$$

Then there is always some location of the sonic point with respect to the cell boundaries for which the cell containing the sonic point does not receive any flux contributions; specifically, this is the case when

$$(\hat{a} + \frac{\delta a}{2})_{I-\frac{1}{2}} < (\hat{a} - \frac{\delta a}{2})_{I+\frac{1}{2}}. \tag{52}$$

This will lead to an expansion shock of some finite strength.

4 Treatment of the Source Term

None of the transonic fluxes derived above will yield a good approximation of a steady transonic expansion if one fails to treat the source term properly. The most dissipative scheme, i.e., the one including (48) as the fan's spread, merely seems to smooth an underlying roughness of the solution over a few cells (see numerical example in next section).

The question is, how to properly split the source term. To answer this, we must go back to the geometry of Figure 1. Assume that z, just as a, varies linearly in the transonic region; we may then define a linear mapping of z onto a:

$$z = z_s + \frac{\delta z}{\delta a} a, \tag{53}$$

where z_s is the source value in the sonic point (see Figure 4). We may define averages $\hat{z}$, $\widehat{z^+}$ and $\widehat{z^-}$ on the full fan, its forward and its backward part, in the same way as previously $\hat{a}$, $\widehat{a^+}$ and $\widehat{a^-}$. This yields, in the first place,

$$\hat{z} = z_s + \frac{\delta z}{\delta a}\hat{a}, \tag{54}$$

or

$$z_s = \hat{z} - \frac{\delta z}{\delta a}\hat{a}, \tag{55}$$

to be used to eliminate z_s; furthermore,

$$\widehat{z^+} = \frac{1}{2}\left[z_s + (\hat{z} + \frac{\delta z}{2})\right] = \hat{z} - \widehat{a^-}\frac{\delta z}{\delta a}, \tag{56}$$

$$\widehat{z^-} = \frac{1}{2}\left[z_s - (\hat{z} - \frac{\delta z}{2})\right] = \hat{z} - \widehat{a^+}\frac{\delta z}{\delta a}, \tag{57}$$

note that

$$\widehat{z^+} + \widehat{z^-} = z_s + \hat{z}, \tag{58}$$

unlike anything we have seen before.

In the steady state, the flux difference must be balanced by the source integral, approximated by $\hat{z}\Delta x$ (see Eq. (12)); we shall split this term in analogy to (20):

$$\hat{z}\Delta x = \widehat{z^+}(\Delta x)^+ + \widehat{z^-}(\Delta x)^-. \tag{59}$$

Here $(\Delta x)^\pm$ denotes the portion of the mesh (x_I, x_I+1) from which the forward/backward characteristics in the fan depart. We therefore have

$$(\Delta x)^+ = \frac{2\widehat{a^+}}{\delta a}\Delta x, \quad (\Delta x)^- = -\frac{2\widehat{a^-}}{\delta a}\Delta x, \tag{60}$$

and we may rewrite the splitting (59) as

$$\hat{z}\Delta x = z^{+*}(\Delta x) + z^{-*}(\Delta x), \tag{61}$$

with

$$z^{+*} = 2\frac{(\widehat{z^+})^2}{\delta z}, \quad z^{-*} = -2\frac{(\widehat{z^-})^2}{\delta z}. \tag{62}$$

The quantities $z^{\pm *}$ may be called the effective source terms for the forward/backward characteristics in the fan; as usual, they add up to $\hat{z}$;

$$z^{+*} + z^{-*} = \hat{z}. \tag{63}$$

We may now define $|z|^*$ as needed to replace $|\hat{z}|$ in the flux function (3):

$$|z|^* = z^{+*} - z^{-*} = \frac{\hat{a}}{\delta a}\left(2\hat{z} - \hat{a}\frac{\delta z}{\delta a}\right) + \frac{\delta z}{4}. \tag{64}$$

Note that if $z_s = 0$, which means that the sonic point already lies in the throat of the channel, we have

$$\hat{z} = \hat{a}\frac{\delta z}{\delta a}, \tag{65}$$

therefore,

$$|z|^* = \frac{\hat{z}^2}{\delta z} + \frac{\delta z}{4}, \tag{66}$$

which is the same formula as for $|a|^*$, cf. Eq. (25).

The significance of the general formula (64), for $z_s \neq 0$, is illustrated in Figure 4. As long as the steady state has not been reached, one will in general find the sonic point away from the throat, i.e., z does not vanish where a vanishes. The splitting of $\hat{z}$ according to (64) guarantees that, when the sonic point approaches its final position, the flux difference and source integral over the positive/negative part of the fan smoothly approach a perfect balance. Another way to achieve detailed balance is to split the source term similarly, but *only in the throat*, regardless of the position of the sonic point. This also works but is somewhat clumsy, as one still has to define *some* kind of splitting of $\hat{z}$ near a sonic point, for use in the flux formula (3). Moreover, this approach will be harder to generalize to multi-dimensional flow, as it requires examining the shape of streamtubes.

5 Numerical Verification

The combination of Eqs. (25) and (64) in the flux function (3), i.e.,

$$f(u_I, u_{I+1}) = \frac{1}{2}\left[f(u_I) + f(u_{I+1})\right] - \frac{1}{2}\sum_k \left[\hat{R}_k\left(|a_k|^*\Delta v_k - |z_k|^*\Delta x\right)\right]_{I+\frac{1}{2}} \tag{67}$$

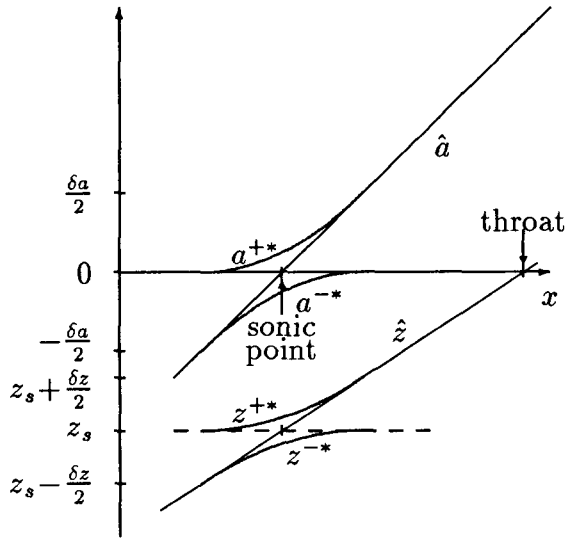

Figure 4: The Entropy Bypass: synchronous splitting of source and characteristic speed near a sonic point. Grid points on the $x-$axis are suppressed; the grid can be arbitrarily shifted with respect to the sonic point.

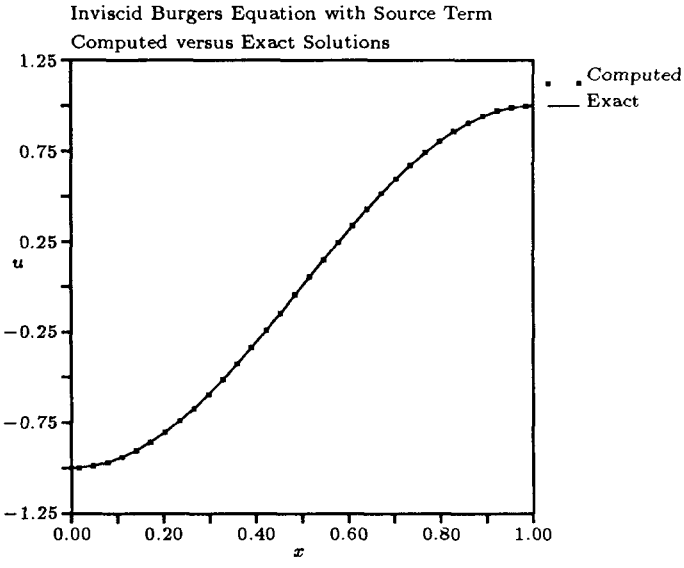

Figure 5: Steady transonic solution of Burgers' equation with source term. Modified transonic flux, with $\delta a = 4\Delta a$, $\delta z = 4\Delta z$. The sonic point, at $x_s = 0$, lies exactly at a cell face.

with $\delta a_k = 4\Delta a_k$, $\delta z_k = 4\Delta z_k$, performed flawlessly in computing steady solutions of both the inviscid Burgers equation and the one-dimensional Euler equations with source terms. The choice $\delta a_k = 2\Delta a_k$, $\delta z_k = 2\Delta z_k$, performed equally well in the simple cases we studied, and yielded almost the identical solutions. Using $\delta a_k = \Delta a_k$, $\delta z_k = \Delta z_k$, however, made the scheme lose a great deal of robustness: unless starting from initial values very close to the correct steady state, the results tended toward an incorrect solution featuring a sonic plateau.

Figure 5 shows the steady solution obtained for Burgers' inviscid equation with a source term, namely,

$$u_t + (\frac{1}{2}u^2)_x = -\frac{\pi}{2}\sin\left[2\pi(x - x_s)\right], \qquad (68)$$

and periodic boundary conditions on the interval $(0, 1)$. The grid is uniform and has 32 cells. The sonic point is given by $x_s = 0$, which coincides with a cell face. The numerical values in the adjacent cells yield a discrete value for $\partial u/\partial x$ of 3.1482, close to the correct value π. Repeating the calculation on finer grids confirms the point-wise second-order accuracy of the solution. The convergence history for the computation of Figure 5 is shown in Figure 6. In all the computations reported in this section, local time-stepping was used.

Figures 7 and 8 show solutions of similar quallity, obtained for different sub-cell locations of the sonic point, namely, $x_s = \Delta x/4$ (Figure 7) and $x_s = \Delta x/2$ (Figure 8).

Figure 9 shows what happens in using Godunov's flux

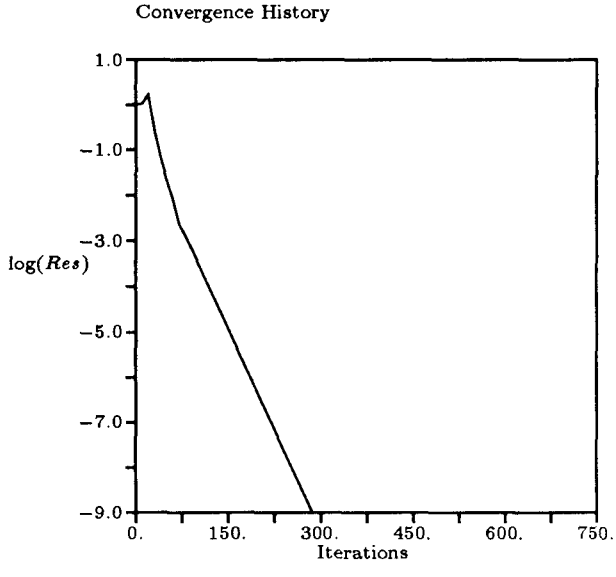

Figure 6: Convergence history for the computation of Figure 5.

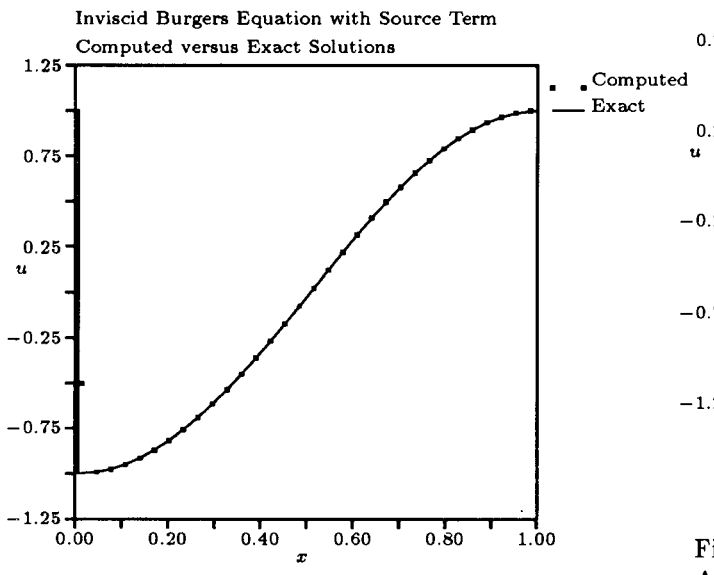

Figure 7: Same as Figure 5, but with $x_s = \Delta x/4$.

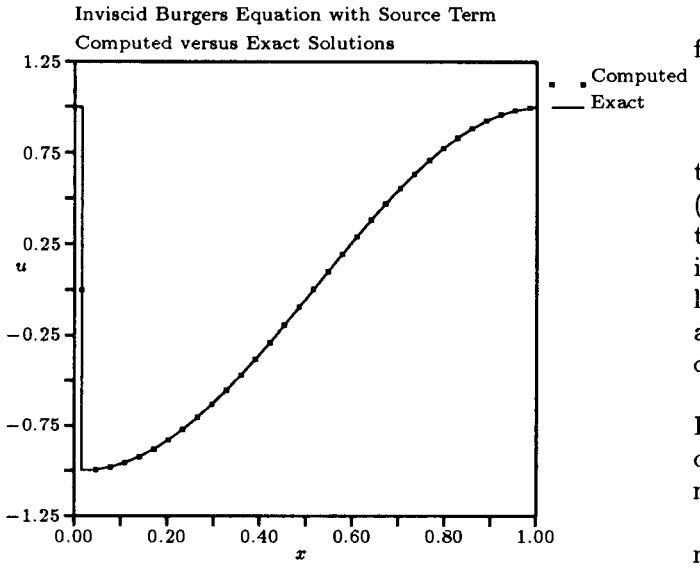

Figure 8: Same as Figure 5, but with $x_s = \Delta x/2$.

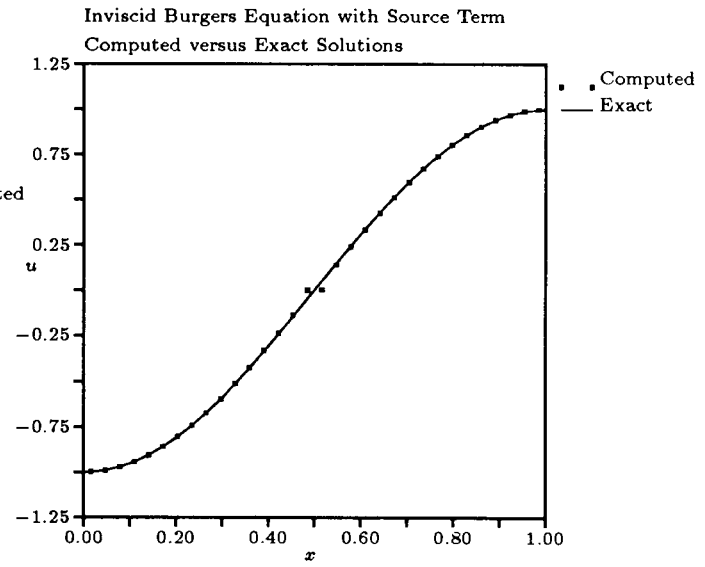

Figure 9: Same as Figure 5, but with $\delta a = \Delta a$, $\delta z = \Delta z$. The results converge slowly to an incorrect solution with a sonic plateau.

with proper treatment of the source term, i.e., $\delta a_k = \Delta a_k$, $\delta z_k = \Delta z_k$, starting from zero initial values. The steady solution with the plateau is very hard to reach, as seen from the convergence history in Figure 10; this suggests that there may actually not be an exact steady discrete solution. The computation may end in a limit cycle (not checked).

Some Euler results are shown in Figures 11-17, for flow in a channel with cross-section

$$D(x) = \frac{3}{2} - \frac{1}{2}\cos(\pi x), \quad -1 \le x \le 1; \qquad (69)$$

the cross-section is constant (=2) outside the interval $(-1, 1)$. Figures 11 and 12 show the Mach-number distribution and convergence history for the flux function incorporating $\delta a_k = 4\Delta a_k$, $\delta z_k = 4\Delta z_k$, for the nonlinear characteristic families, i.e., $k = 1,\ 3$. Again, the agreement with the exact solution is point-wise second-order.

The robustness of the Entropy Bypass is shown in Figures 13 and 14, in which oscillatory initial conditions, with multiple sonic-points, are given. The method converges rapidly to the exact solution.

Figure 15 shows what one loses if the source term is not treated according to Eq. (64). In this case we used

$$|\hat{z_k}| := \frac{2\hat{a}_k}{\delta a_k}\hat{z}_k, \quad k = 1,\ 3, \qquad (70)$$

with considerable loss of accuracy.

Finally, Figure 16 is based on the Godunov-like flux, with proper source-term treatment, i.e., $\delta a_k = \Delta a_k$, $\delta z_k = \Delta z_k$, $k = 1, 3$. The linear initial-value distribution indicated in the figure ended up,

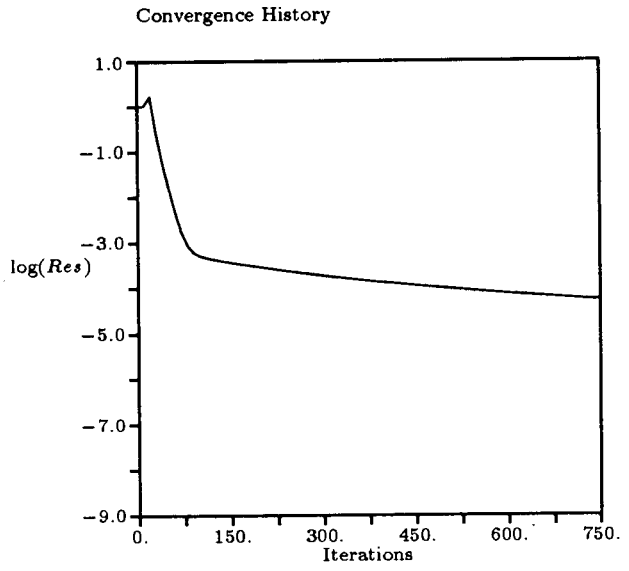

Figure 10: Convergence history for the computation of Figure 9.

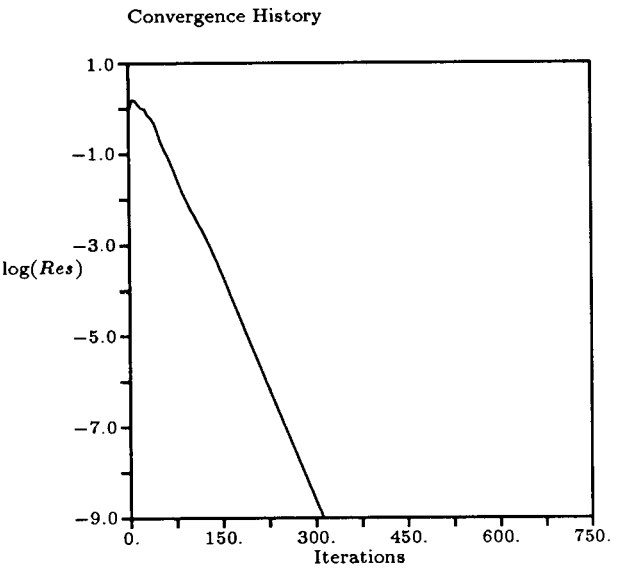

Figure 12: Convergence history for the computation of Figure 11.

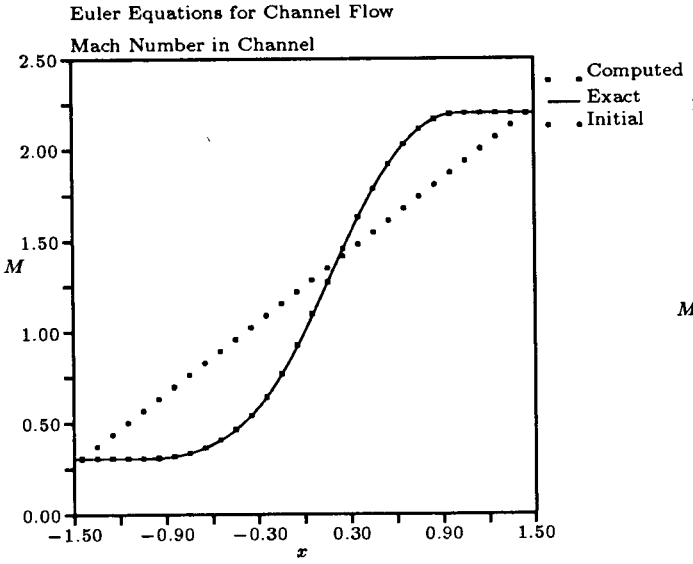

Figure 11: Transonic solution of the Euler equations for flow in a converging-diverging channel; shown are Mach-number distributions. Modified flux, with $\delta a_k = 4\Delta a_k$, $\delta z_k = 4\Delta z_k$, $k = 1, 3$.

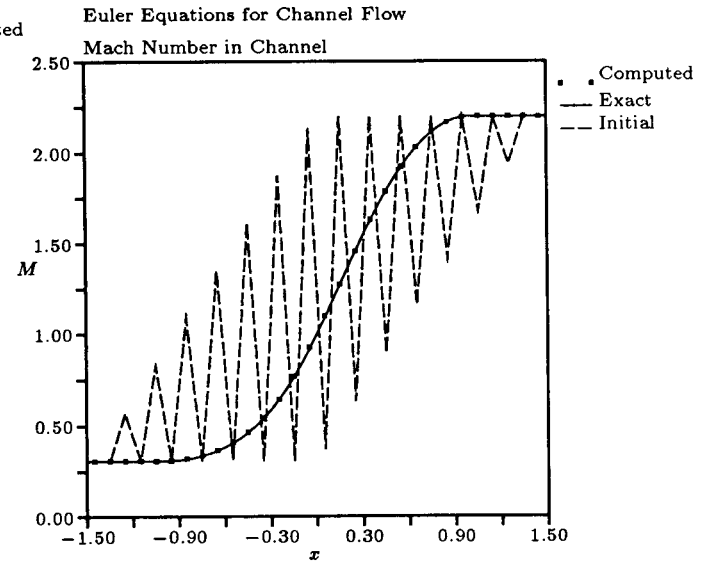

Figure 13: Same as Figure 11, but with multiple sonic-points in the initial distribution.

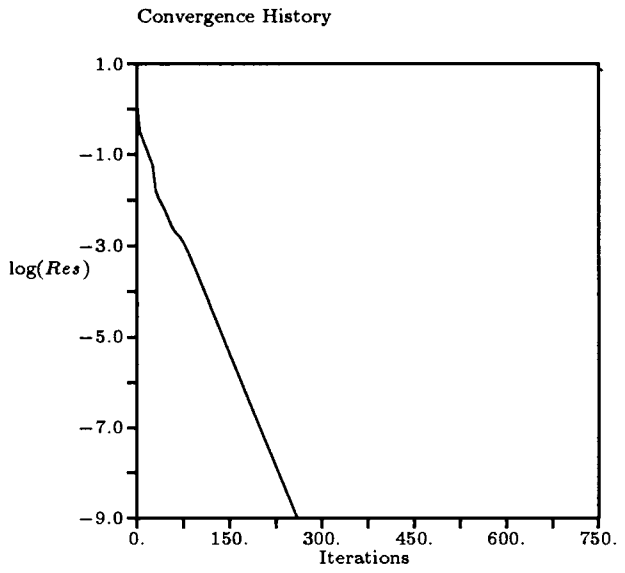

Figure 14: Convergence history for the computation of Figure 13.

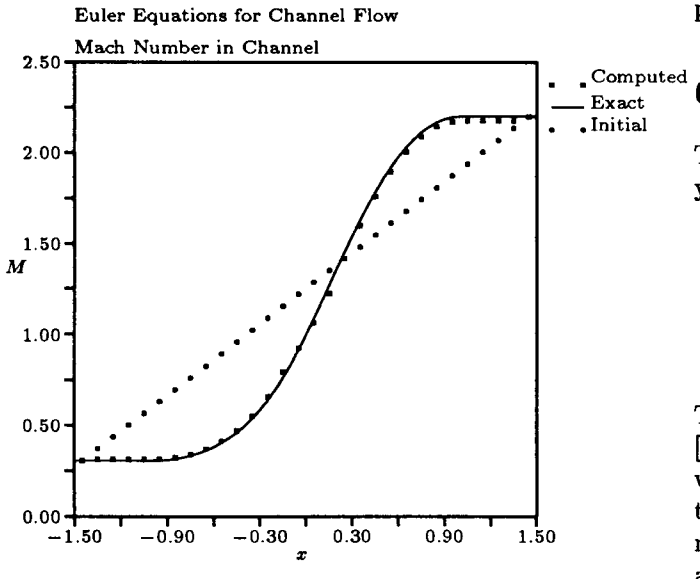

Figure 15: Same as Figure 11, but with incorrect source-term splitting, viz.: $|\hat{z}| := \hat{z}(2\hat{a}/\delta a)$.

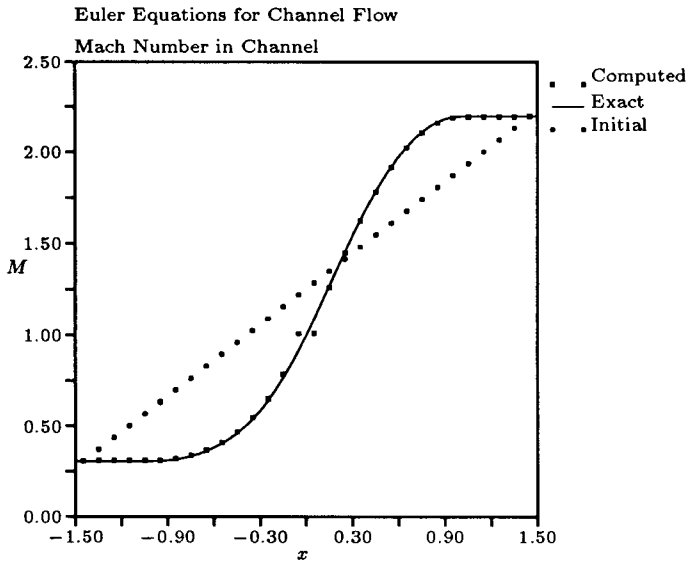

Figure 16: Same as Figure 11, but with $\delta a_k = \Delta a_k$, $\delta z_k = \Delta z_k$, $k = 1, 3$. Starting from straight-line initial values, an incorrect solution with a sonic plateau is slowly established.

as for Burgers' equation, in a solution with a sonic plateau. The associated slow convergence can be seen from Figure 17. If, on the other hand, one provides this Godunov-like scheme with the steady solution from Figure 11 as initial-value distribution, it will essentially preserve it.

6 Conclusions and Perspective

The analysis in Sections 2-4 has, among other things, yielded the following results:

- a numerical flux function for use near a sonic point, based on a full model of a transonic expansion wave;
- a matched treatment for the source term.

The flux formula turns out to be identical to Harten's [12] ad hoc formula. It contains a free parameter by which the rate of spreading of the expansion fan, i.e., the dissipation, can be controlled. For optimal robustness in time marching, this parameter should be given a value equal to four times the nominal value that follows from the model; this follows from the analysis of Goodman and LeVeque [13].

Numerical results confirm the correctness of the analysis. With the proper flux splitting and source splitting, the first-order upwind scheme of Roe [14] and Van Leer [8] produces pointwise second-order-accurate steady transonic solutions of the Burgers and Euler equations, without transonic jumps or plateaus.

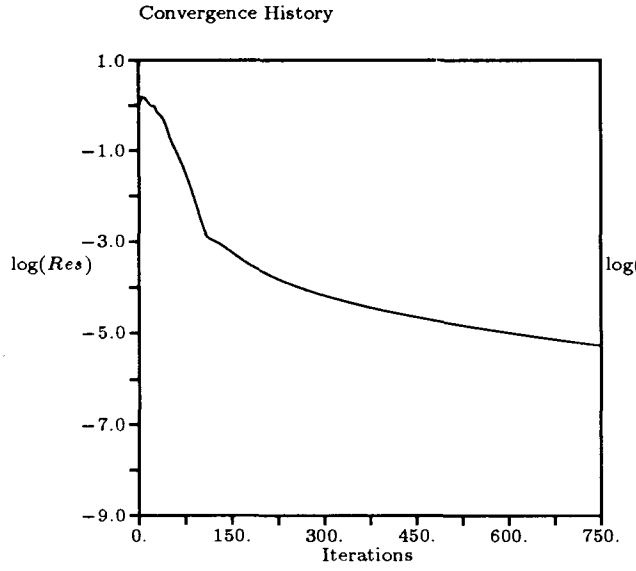

Figure 17: Convergence history for the computation of Figure 16.

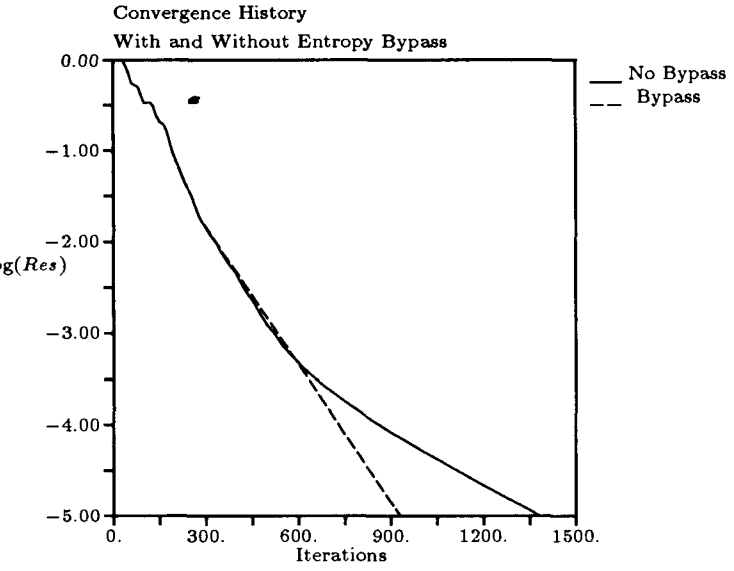

Figure 18: Convergence history for two-dimensional computations of transonic channel flow, (a) using an entropy-violating flux, (b) using an entropy-satisfying flux.

It must be emphasized that the above analysis applies exclusively to finite-volume schemes for computing steady solutions. For such schemes, what matters most is the proper balance, near a sonic point, of flux-differences and source terms. This yields the desired accuracy in the steady state; for the sake of robustness we've had to concern ourselves to some extent with temporal accuracy near a sonic point. The transonic flux derived, however, is *not* the full answer to the question of designing a scheme that maintains temporal accuracy in the vicinity of a sonic point; this was pointed out by Roe [17]. Future publications of Roe and the present authors may address this question in detail.

The extension of the one-dimensional analysis to multi-dimensional flows appears straightforward, if an auxiliary flow-aligned coordinate system is adopted. The two-dimensional Euler equations, for instance, can be written as

$$u_t + f_\xi + g_\eta = 0, \qquad (71)$$

where ξ measures length in the streamwise direction and η in the normal direction; the η-derivative of the normal flux g may be regarded here as a source term that determines the cross-section of the streamtube, and may be treated as in the one-dimensional case. One thus ends up with fluxes in a coordinate system rotated with respect to the grid lines; the fluxes needed for advancing the solution on the grid are then obtained by the inverse of this rotation. Implementation of this quasi-one-dimensional technique is presently under way.

It has been observed that multi-dimensional flows are more forgiving as regards the numerical treatment of sonic points than one-dimensional flows. An expansion shock, for instance, is easily generated in a one-dimensional calculation through the use of a numerical flux function like (39), violating the entropy condition. In two dimensional calculations, though, expansion shocks appear to be destroyed by transverse waves. Yet, the desire of the numerical solution to derail may be evident from a deterioration of the convergence toward the steady state. An example of loss of convergence because of an "entropy-violating" flux function is given in Figure 18. The flow computed is the two-dimensional equivalent of the case of Figure 11, i.e., transonic flow in a converging-diverging channel. The entrance Mach number for the case was $M_\infty = 0.47$. The channel had a 20% constriction, and the grid was 45×15. The stagnating residual-convergence curve is for the entropy-violating flux; the fully converging residual corresponds to the numerical flux function discussed in Section 3 (no source term included).

The example of Figure 18 suggests that there is a lot to gain from extending the present analysis to multi-dimensional flows. That, of course, will be the subject of a sequel paper.

Acknowledgements

The research reported in this paper was funded in part by the National Science Foundation under Grant EET-8857500, monitored by Dr. George Lea, and by the National Aeronautics and Space Administration under Grant NAG-1-869, monitored by Dr. James Thomas of NASA Langley Research Center.

The authors are indebted to Phil Roe for the flux

normalization defined in Equations (49) and (50) and used in Figure 3.

References

[1] P. L. Roe and B. van Leer, "Non-existence, non-uniqueness and slow convergence of discrete hyperbolic conservation laws." Presented at the Third Conference on Numerical Methods for Fluid Dynamics, 1988.

[2] T. J. Barth, "Some notes on perfect shock resolving flux function — Part 1: Stationary characteristics," NASA TM 101087, 1989.

[3] P. R. Woodward and P. Colella, "The numerical simulation of two-dimensional fluid flow with strong shocks," *Journal of Computational Physics*, vol. 54, pp. 115–173, 1984.

[4] T. W. Roberts, "The behavior of flux difference splitting schemes near slowly moving shock waves." Presented at the Third Conference on Numerical Methods for Fluid Dynamics, Oxford, 1988.

[5] P. L. Roe, "A survey of upwind differencing techniques." Invited Lecture at the Eleventh International Conference on Numerical Methods in Fluid Dynamics, 1988.

[6] S. F. Davis, "A rotationally-biased upwind difference scheme for the Euler equations," *Journal of Computational Physics*, vol. 56, 1984.

[7] D. Levy, K. G. Powell, and B. van Leer, "Implementation of a grid-independent upwind scheme for the Euler equations," in *AIAA 9th Computational Fluid Dynamics Conference*, 1989.

[8] B. van Leer, "On the relation between the upwind-differencing schemes of Godunov, Engquist-Osher and Roe," *SIAM Journal on Scientific and Statistical Computing*, vol. 5, 1984.

[9] P. Colella, "Glimm's method for gas dynamics," *SIAM Journal on Numerical Analysis*, vol. 18, pp. 289–315, 1981.

[10] S. Osher and S. K. Chakravarthy, "Upwind schemes and boundary conditions with applications to Euler equations in general geometries," *Journal of Computational Physics*, vol. 50, 1983.

[11] B. van Leer, "Towards the ultimate conservative difference scheme. V. A second-order sequel to Godunov's method," *Journal of Computational Physics*, vol. 32, 1979.

[12] A. Harten, "High-resolution schemes for hyperbolic conservation laws," *Journal of Computational Physics*, vol. 49, pp. 357–393, 1983.

[13] J. B. Goodman and R. J. LeVeque, "A geometric approach to high resolution TVD schemes," *SIAM Journal on Numerical Analysis*, vol. 25, 1988.

[14] P. L. Roe, "Characteristic-based schemes for the Euler equations," *Annual Review of Fluid Mechanics*, vol. 18, pp. 337–365, 1986.

[15] S. K. Godunov, "A finite-difference method for the numerical computation and discontinuous solutions of the equations of fluid dynamics," *Matematicheskii Sbornik*, vol. 47, pp. 271–306, 1959.

[16] S. Osher, "Riemann solvers, the entropy condition and difference approximations," *SIAM Journal on Numerical Analysis*, vol. 21, pp. 217–235, 1984.

[17] P. L. Roe, "A note on sonic-point fluxes." Private Communication, 1989.